

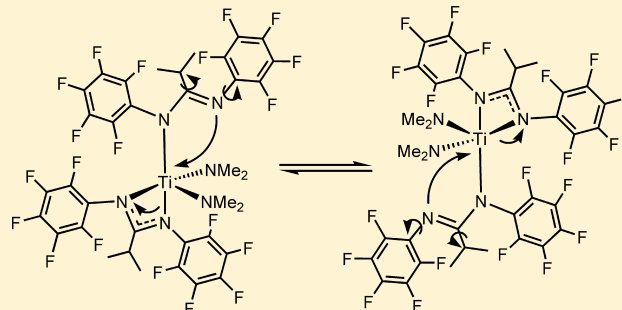
Synthesis and Characterization of Group 4 Fluorinated Bis(amidinates) and Their Reactivity in the Formation of Elastomeric Polypropylene

Tatyana Elkin, Sinai Aharonovich, Mark Botoshansky, and Moris S. Eisen*

Schulich Faculty of Chemistry, Technion—Israel Institute of Technology, Haifa 32000, Israel

Supporting Information

ABSTRACT: Bis(amidinate) titanium and zirconium bis(dimethylamido) complexes were prepared, and the dynamic behavior of the titanium complex containing perfluorinated amidinate ligand (**11**) was studied in detail. The variable-temperature NMR revealed the presence of two species in solution, in line with the different connection modes of the ligand to the metal center. The resulting complexes were tested as catalysts in the polymerization of propylene, and the resulting polymers were consistent with elastomeric high-molecular-weight atactic polypropylenes.



INTRODUCTION

In the last two decades, the search for new polymeric materials and specially polyolefins with valuable physical and mechanical properties has seen impressive growth. Considerable attention was drawn to the design and synthesis of homogeneous nonmetallocene group IV catalysts, which have reached a high level of sophistication.^{1–3} Polypropylene is among the most commercially important polyolefins, with a worldwide production of ca. 4×10^7 tons/y, about 6 kg per capita in 2006, with an additional 17% growth expected until 2020.¹ Catalysts generated from early-transition-metal complexes containing the amidinate ligands $[NR^1CR^2NR^3]^-$ have been found to be active in the polymerization of α -olefins. The amidinates are attractive ancillary ligands due to their rich coordination chemistry, their facile synthesis, and the opportunity to tune their electronic and steric properties.^{4–6} We have shown that when the bis(*p*-arylamidinate) group 4 dichloride/dialkyl complexes are activated by methylaluminoxane (MAO), the resulting active species polymerize propylene, affording a mixture of two polypropylene fractions: a minor isotactic fraction and a nonstereospecific elastomeric fraction. These two fractions are obtained by a bis(*p*-arylamidinate) group 4 cationic monoalkyl complex and a corresponding cationic mono(*p*-arylamidinate) group 4 complex, respectively.⁷ Mechanistic studies have suggested that the mono(*p*-arylamidinate) titanium trialkyl complex is obtained via the dynamic behavior of the arylamidinate ligands, resulting in the migration of one of the two amidinate ligands to MAO.^{7a,8} This new highly coordinatively unsaturated complex responds to the ligand migration by rearranging the additional (*p*-arylamidinate) ligand, resulting in the reattachment of the ligand to the metal via one nitrogen atom and a π -bonded phenyl ring (Scheme 1). We have shown that, when comparing the simple

bis(phenylamidinate) titanium dichloride to the bis(*p*-tolylamidinate) titanium dichloride complex, a polypropylene with much higher molecular weight and a complex with a reduced catalytic activity are obtained in the latter case, thus corroborating our observations.⁹ This substituent effect is extraordinary in view of the distant location of the *para* substituent from the active metal center in the κ^2 -bonded amidinate, which precludes significant steric, inductive, field, or resonance effects and supports the observed ligand rearrangement (Scheme 1).

In addition to the benzamidinates, myriads of ancillary ligands have attracted considerable attention in the last 25 years, and in combination with transition metals, designed complexes have been obtained for the catalytic polymerization of α -olefins.^{3,10} One type of these elegant ligands that has attracted our attention is the phenoxyimine ligands and their corresponding group 4 catalysts (FI catalysts). The use of these complexes in the polymerization of ethylene containing a fluorine atom at the ortho position of the *N*-aryl moiety surprisingly led to a living polymerization.¹¹ On the basis of theoretical studies it was suggested that the chain termination is avoided due to the preferential F···H interaction between the fluorine atom of the ancillary ligand and a β -hydrogen of the growing polymer chain.¹² Interestingly, the suppression of a β -hydride chain transfer was observed very recently in a Ni(II) complex in the polymerization of ethylene due to a weak fluorocarbon ligand–product interaction.^{12d}

Hence, it was conceptually interesting to study if such a unique interaction can also be applied to fluorinated amidinate ligands. We present herein the preparation of various Ti and Zr complexes decorated with several *N*-fluoroaryl amidinates, their

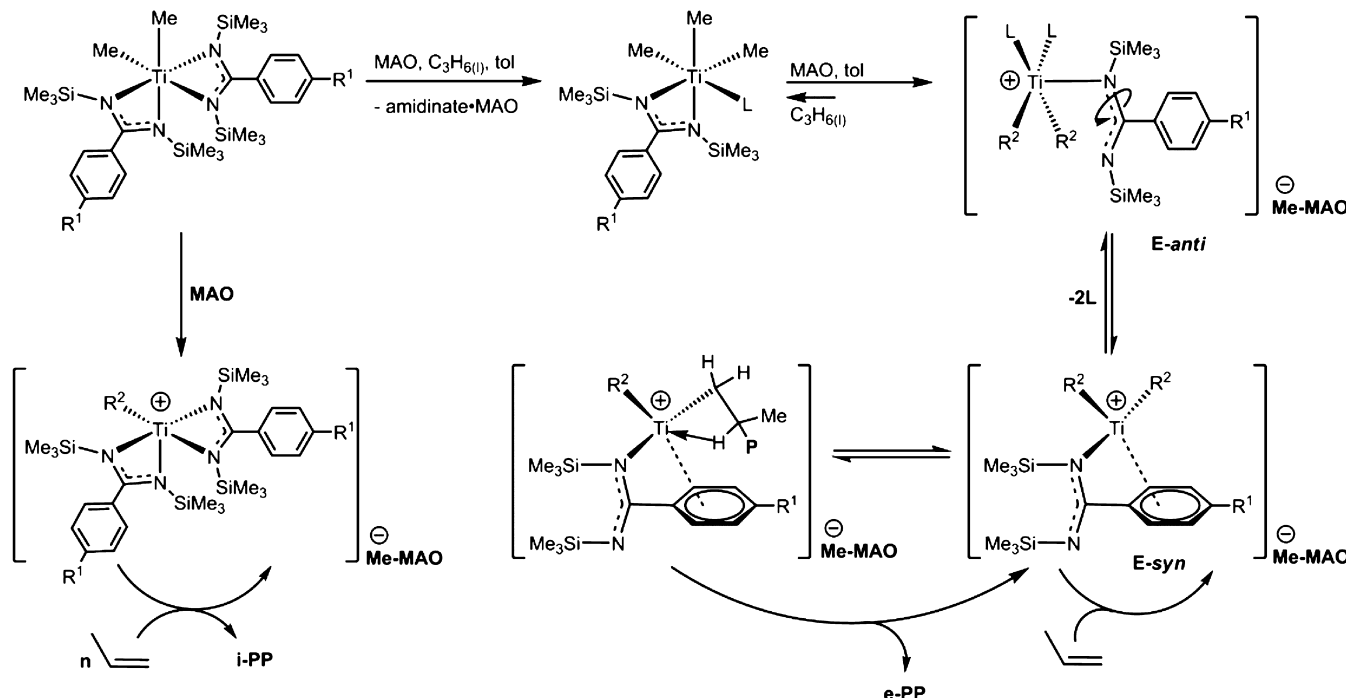
Received: July 25, 2012

Published: October 18, 2012



ACS Publications

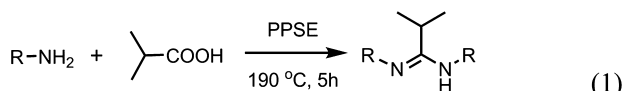
© 2012 American Chemical Society

Scheme 1. Active Species Formed during the Activation of Titanium Bis(*p*-arylamidinate) Dichloride Complex with MAO

solution and solid-state structures, and their propylene polymerization behavior.

RESULTS AND DISCUSSION

We start the presentation of the results by disclosing why the specific ligands were designed for this study. We have recently shown (Scheme 1)⁹ that in the cationic mono aryl/phenyl amidinate complexes the aromatic ring will rearrange, producing a κ^6 coordination structure and any substituent at the *para* position will interact with a growing polymer chain, retarding a chain transfer and allowing higher molecular weights (the bigger the substituent, the larger the molecular weight of the obtained polymer). This is a steric effect of the *para* substituent exhibiting a linear free energy relationship with the Taft parameter. Hence, to eliminate any π bonding of the aryl/phenyl amidinate ring while keeping the steric environment similar to that of the arylamidinates, the ligands were prepared with an isopropyl moiety, instead of the aryl group, at the amidine carbon substituent. In addition, a range of differently fluorinated aromatic rings were used as the amidinate nitrogen substituents. The amidines were synthesized using polyphosphoric acid trimethylsilyl esters (PPSE) as the condensation reagent (eq 1).¹³



$\text{R} = \text{C}_6\text{H}_5$ (1), *m*-F-C₆H₄ (2), *p*-F-C₆H₄ (3), 8-F-C₁₀H₁₆ (4)

Our first attempts to prepare the ligand containing the pentafluorophenyl ring by the condensation of the aniline with the corresponding acyl chloride and the concomitant condensation of the resulting amide with an additional 1 equiv of pentafluoroaniline, led to very low yields (2–5%) of the desired amidine 5. Full conversion toward the desired amidine 5 (30% isolated yield) and the corresponding

imidazole 6 (70% isolated yield) were obtained (Scheme 2) in the condensation of pentafluoroaniline with isobutyric acid, in the presence of PPSE.¹³ Interestingly, we have found that the order of addition of the reagents to the reaction mixture has a dramatic influence on the obtained ratio for the two products. If the pentafluoroaniline is added first to the PPSE, the imidazole 6 is the only observed product, isolated in 96% yield. However, if the isobutyric acid is added first to the PPSE, followed by the addition of the pentafluoroaniline, a mixture of the amidine 5 and the imidazole 6 is obtained. Addition of a slight excess of isobutyric acid (beyond 1 equiv) results in the production of the corresponding amide and the imidazole without formation of the amidine. These results indicate that the amide can be attacked by the amine either at the carbonyl group, affording the amidine 5, or at the ortho position of the C₆F₅ ring, removing a fluorine atom followed by an intramolecular ring closure to form the imidazole 6. Interestingly, a mixture of the amidine with PPSE does not produce imidazole.

Perspective views of the molecular structures of the amidines 3–5 and the corresponding imidazole 6 are presented in Figures 1–4, respectively. Notably, the methyl groups of the isopropyl moiety are disposed in the solid structure to minimize interactions with any nearby fluorine atoms. In addition, the isopropyl group forms a dihedral angle with the N–C–N plane, C15–C14–C13–N2 = 57.79 and 50.28° and C16–C14–C13–N2 = 68.34 and 72.84°, for ligand 5 and compound 6, respectively, similarly to the arylamidinates (vide infra). As can be observed for all the amidine ligands, the NH–C(central) and the N=C bond lengths and the N=C–NH bond of all of the amidine ligands are alike, exhibiting no major differences.

Several titanium and zirconium complexes were prepared by the reaction of 1 equiv of either Ti(NMe₂)₄ or Zr(NMe₂)₄ metal precursor with 2 equiv of the corresponding neutral amidines (eq 2). For the corresponding titanium complexes (7, 9, and 11) and the zirconium complex (12) X-ray crystallo-

Scheme 2. Synthesis of the Bis(pentafluorophenyl) Isopropyl Amidinate Ligand 5 and the Corresponding Benzimidazole 6

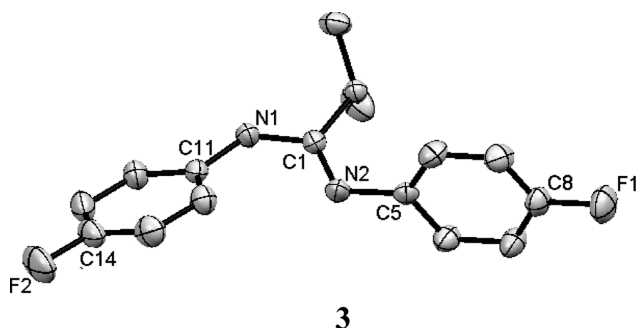
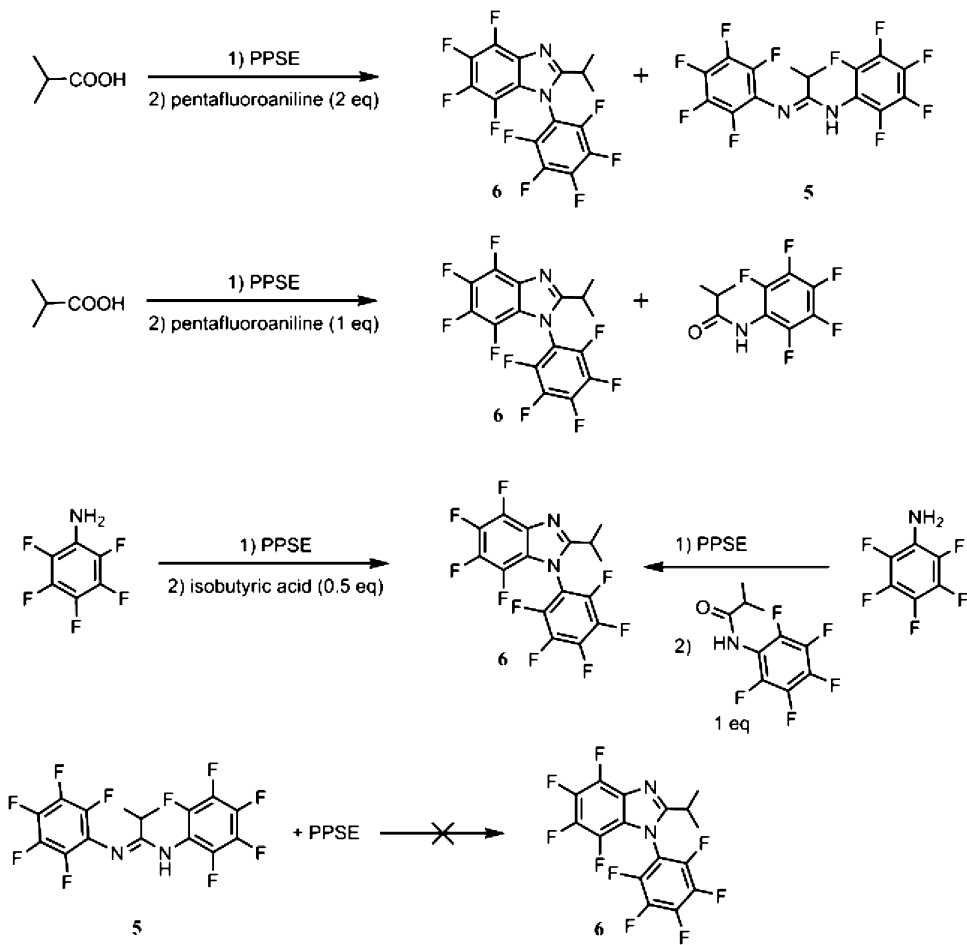


Figure 1. Mercury diagram of the molecular structure of amidine 3 (25% probability ellipsoids). Hydrogen atoms are omitted for clarity. Representative bond lengths (\AA) and angles (deg): C(1)–N(1) = 1.362(2); C(1)–N(2) = 1.287(2); C(11)–N(1) = 1.416(2); C(5)–N(2) = 1.418(2); C(14)–F(2) = 1.366(3); C(8)–F(1) = 1.360(2); N(2)–C(1)–N(1) = 119.85(16).

graphic studies were performed, and the Mercury diagrams are presented in Figures 5–8, respectively.

In the solid state, complexes 7, 9, 11, and 12 all exhibit C_2 symmetry, where the metal is situated in a pseudo-octahedral environment that is formed by four nitrogen atoms from the amidinate ligands and two nitrogen atoms from the dimethylamido groups. In these complexes, the dimethylamido groups are disposed in a *cis* position, and the M–N bond lengths of the dimethylamido moieties (1.893(2) and 1.899(2) \AA for complex 7, 1.893(5) and 1.898(5) \AA for complex 9, and

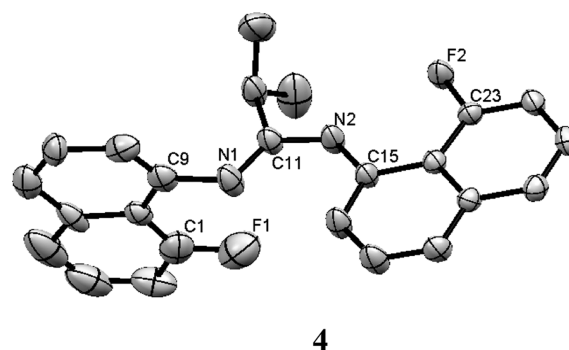


Figure 2. Mercury diagram of the molecular structure of amidine 4 (25% probability ellipsoids). Hydrogen atoms are omitted for clarity. Representative bond lengths (\AA) and angles (deg): C(11)–N(1) = 1.374(4); C(11)–N(2) = 1.268(4); C(9)–N(1) = 1.408(4); C(15)–N(2) = 1.422(4); C(1)–F(1) = 1.380(4); C(23)–F(2) = 1.356(4); N(2)–C(1)–N(1) = 120.9(3).

1.889(5) and 2.031(3) \AA for complexes 11 and 12, respectively) are shorter, as expected, than the M–N bond lengths of the coordinated amidinate (2.1018(18), 2.1769(19), 2.091(2), and 2.222(2) \AA for complex 7, 2.120(5), 2.214(5), 2.105(5), and 2.234(5) \AA for complex 9, 2.124(6) and 2.247(5) \AA for complex 11, and 2.242(3) and 2.341(3) \AA for complex 12, respectively). These latter M–N bond lengths are comparable to those found in previously reported amidinate complexes.¹⁴

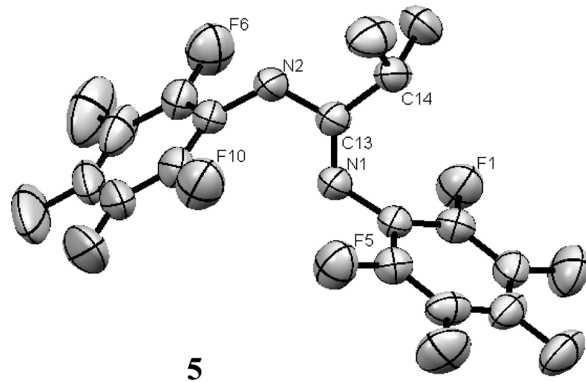


Figure 3. Mercury diagram of the molecular structure of the amidine **5** (25% probability ellipsoids). Hydrogen atoms are omitted for clarity. Representative bond lengths (\AA) and angles (deg): C(13)–N(1) = 1.277(3); C(13)–N(2) = 1.376(3); C(1)–N(1) = 1.399(3); C(7)–N(2) = 1.404(3); C(8)–F(6) = 1.343(4); C(12)–F(10) = 1.337(4); C(2)–F(1) = 1.345(1); C(6)–F(5) = 1.349(3); N(2)–C(13)–N(1) = 117.8(2).

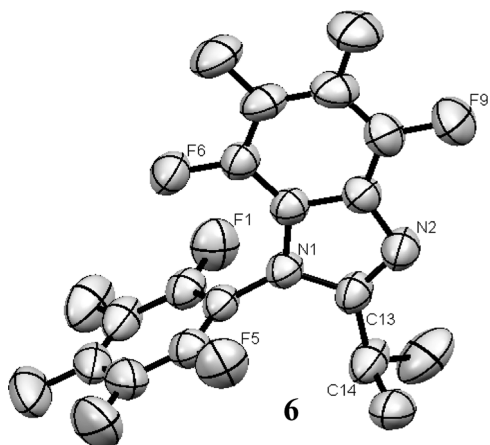


Figure 4. Mercury diagram of the molecular structure of the amidine **6** (25% probability ellipsoids). Hydrogen atoms are omitted for clarity. Representative bond lengths (\AA) and angles (deg): C(13)–N(1) = 1.397(3); C(13)–N(2) = 1.297(3); C(1)–N(1) = 1.412(3); C(7)–N(1) = 1.388(3); C(8)–F(6) = 1.353(3); C(11)–F(9) = 1.348(3); C(2)–F(1) = 1.334(3); C(6)–F(5) = 1.335(3); N(2)–C(13)–N(1) = 112.4(2).

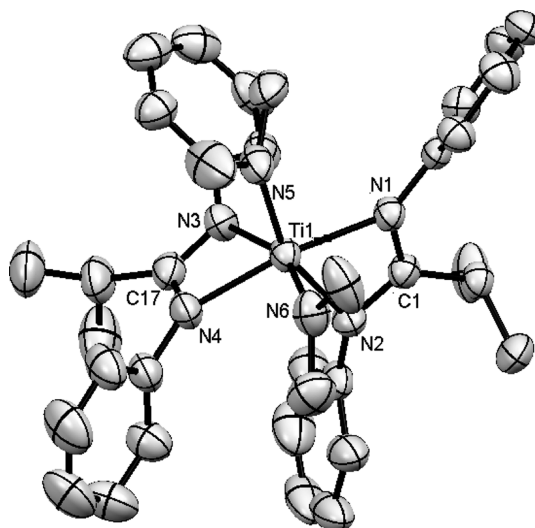
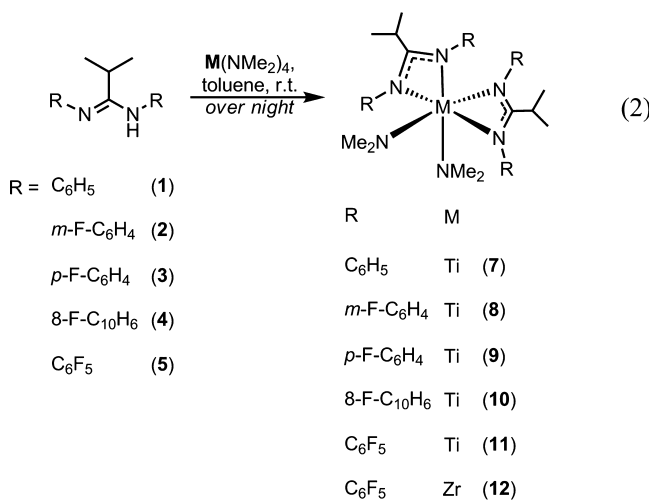


Figure 5. Mercury diagram of the molecular structure of complex **7** (25% probability ellipsoids). Hydrogen atoms are omitted for clarity. Representative bond lengths (\AA) and angles (deg): Ti(1)–N(1) = 2.1018(18); Ti(1)–N(2) = 2.1769(19); Ti(1)–N(5) = 1.893(2); Ti(1)–N(4) = 2.091(2); Ti(1)–N(3) = 2.222(2); Ti(1)–N(6) = 1.899(2); C(1)–N(1) = 1.340(3); C(1)–N(2) = 1.312(3); C(17)–N(3) = 1.308(3); C(17)–N(4) = 1.330(3); N(2)–Ti(1)–N(1) = 60.92(7); N(1)–Ti(1)–N(5) = 94.84(8); N(4)–Ti(1)–N(6) = 96.97(10); N(1)–Ti(1)–N(2)–C(1) = 0.01; N(4)–Ti(1)–N(3)–C(17) = 2.09.

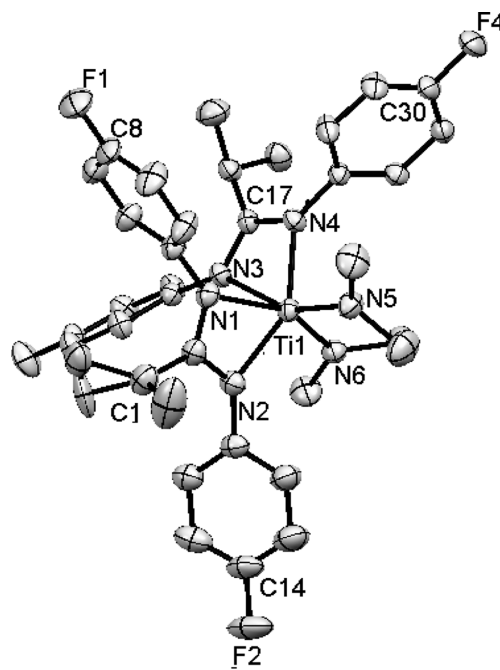


Figure 6. Mercury diagram of the molecular structure of complex **9** (25% probability ellipsoids). Hydrogen atoms are omitted for clarity. Representative bond lengths (\AA) and angles (deg): Ti(1)–N(1) = 2.214(5); Ti(1)–N(2) = 2.120(5); Ti(1)–N(5) = 1.893(5); Ti(1)–N(4) = 2.105(5); Ti(1)–N(3) = 2.234(5); Ti(1)–N(6) = 1.898(5); C(1)–N(1) = 1.322(7); C(1)–N(2) = 1.344(7); C(17)–N(3) = 1.334(7); C(17)–N(4) = 1.350(7); N(2)–Ti(1)–N(1) = 60.55(17); N(1)–Ti(1)–N(5) = 91.3(2); N(3)–Ti(1)–N(6) = 103.6(2); N(1)–Ti(1)–N(2)–C(1) = 2.23; N(4)–Ti(1)–N(3)–C(17) = 3.07.

The shortest distances between an *o*-F atom and the metal center in complexes **11** and **12** exceed the sum of their

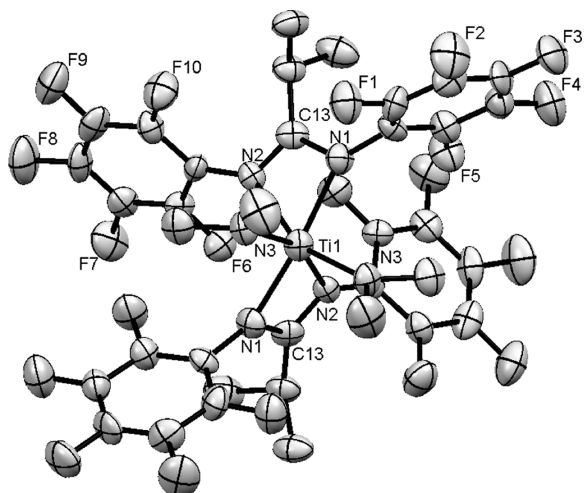


Figure 7. Mercury diagram of the molecular structure of complex **11** (25% probability ellipsoids). Hydrogen atoms are omitted for clarity. Representative bond lengths (\AA) and angles (deg): $\text{Ti}(1)-\text{N}(1) = 2.124(6)$; $\text{Ti}(1)-\text{N}(2) = 2.247(5)$; $\text{Ti}(1)-\text{N}(3) = 1.889(5)$; $\text{C}(13)-\text{N}(1) = 1.356(8)$; $\text{C}(13)-\text{N}(2) = 1.289(8)$; $\text{F}(10)-\text{Ti}(1) = 4.546$; $\text{N}(2)-\text{Ti}(1)-\text{N}(1) = 59.5(2)$; $\text{N}(2)-\text{Ti}(1)-\text{N}(3) = 90.90(2)$; $\text{N}(2)-\text{Ti}(1)-\text{N}(1)-\text{C}(13) = 4.78$.

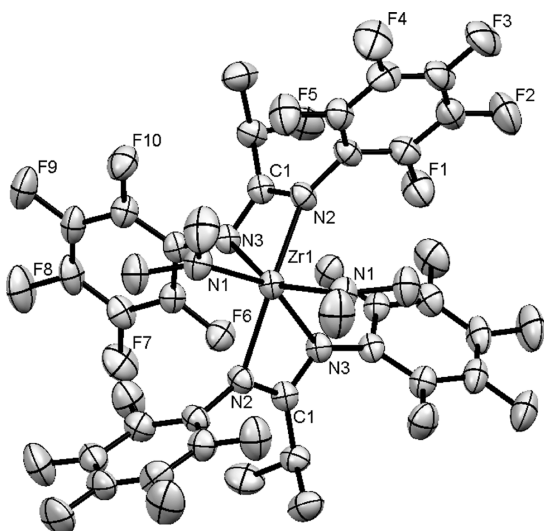


Figure 8. Mercury diagram of the molecular structure of complex **12** (25% probability ellipsoids). Hydrogen atoms are omitted for clarity. Representative bond lengths (\AA) and angles (deg): $\text{Zr}(1)-\text{N}(2) = 2.242(3)$; $\text{Zr}(1)-\text{N}(3) = 2.341(3)$; $\text{Zr}(1)-\text{N}(1) = 2.031(3)$; $\text{C}(1)-\text{N}(2) = 1.351(4)$; $\text{C}(1)-\text{N}(3) = 1.331(4)$; $\text{F}(5)-\text{Zr}(1) = 3.947$; $\text{N}(2)-\text{Zr}(1)-\text{N}(3) = 56.78(9)$; $\text{N}(2)-\text{Zr}(1)-\text{N}(1) = 94.65(11)$; $\text{N}(2)-\text{Zr}(1)-\text{N}(3)-\text{C}(1) = 6.62$.

corresponding van der Waals radii (4.546 \AA in complex **11** and 3.947 \AA in complex **12**),¹⁵ indicating the absence of any notable interaction between the metal center and the F atoms of the fluorinated aryl substituents.

Despite their similar solid-state structures, complexes **11** and **12** display a completely different behavior in solution. In the ^{19}F NMR of complex **12**, only three signals are observed, and in the ^1H NMR only one set of signals corresponding to the isopropyl moieties is detected. The persistence of these observations even at low temperatures (-50°C precipitating temperature of the complex) indicates that a rapid dynamic behavior of the complex **12** (from Δ to Λ via an open–close

ligand mechanism) is operative even at low temperatures. Interestingly, for the rest of the complexes the same rapid dynamic behavior was also observed at low temperatures. From the crystal structure it is apparent that a significant barrier to the rotation of the pentafluorophenyl ring exists in both complexes, since the overlap of the *o*-F with the methyl groups of the isopropyl moiety; however, this interaction is observed only for complex **11**. For complex **11**, a very informative and complex comprehensive spectrum in both ^1H and ^{19}F NMR is obtained at low temperature. The dynamic process for complex **11** was studied with variable-temperature ^{19}F and ^1H measurements, and the respective spectra are presented in Figures 9 and 10.

The outcome of the variable-temperature NMR analysis (^1H , ^{19}F) indicates that only two species (**11A,B**) are present in solution and their ratio, in addition to the different temperature measurements, is kept constant (Figures 9–11 and Table 1). Complex **11A** shows a dynamic behavior as a function of the temperature, whereas complex **11B** exhibits no dynamic behavior in solution over the examined temperature range. From the line broadening analysis, complex **11A** exhibits the dynamic processes (i) rotation of the methyl groups within each isopropyl group and (ii) dynamic equilibration of the isopropyl groups between the two amidinate ligands within the complex with the thermodynamic value measured of $\Delta H^\ddagger = 13.4(0.4)$ kcal mol $^{-1}$ (see the corresponding Eyring plot in the Supporting Information), together with the equilibration of the perfluorinated aromatic rings. Hence, it seems plausible that complex **11A** has one open ligand (κ^1) and one closed chelated ligand (κ^2), whereas in complex **11B** both ligands are connected to the metal center in a κ^2 fashion (at high temperature a broadening of all the spectra lines is appreciable, suggesting a high energy of activation toward the interconversion of **11A** to **11B**). The two complexes **11A,B** were characterized by ^1H and ^{19}F COSY at 227 K (Figures 11 and 12) and also at 365 K (see the Supporting Information). It is important to point out that the presence of the symmetric C_{2v} complex **11**, having two κ^1 chelating ligands, was not observed in solution even when one crystal was dissolved (based on the ^1H and ^{19}F NMR correlating data). In the ^1H NMR at 365 K the signals were broadened, and no final product (coalescence process/correlation among the two complexes) was obtained. Heating beyond 365 K induces a rapid decomposition of the complexes. It is very interesting to follow the signals of the isopropyl moieties in both complexes, showing a nice crossover of the signals, which are also verified in the COSY spectra at the different temperatures. The ratio among the complexes **11A,B** is maintained constant, 70:30, respectively, regardless of the temperature, as was confirmed by both the ^1H and ^{19}F NMR (see the integration of signals in Table 1). The variable-temperature ^{19}F NMR spectra were very informative, and full assignment of the two complexes was possible via their chemical shifts, 2D correlations at the different temperatures, and the corresponding integrations. It is important to point out that two possible geometrical isomers (*cis* and *trans* isomers) could be responsible for the signals obtained in complex **11A** as presented in Figure 11. Our attempts to obtain crystals of just **11A** were unsuccessful; however, for the *trans* isomer a high energy of activation toward its equilibration to complex **12** would be expected.

All of the complexes were tested as suitable catalysts for the polymerization of propylene. Catalytically active species were generated by the reaction of the complexes with methyl-

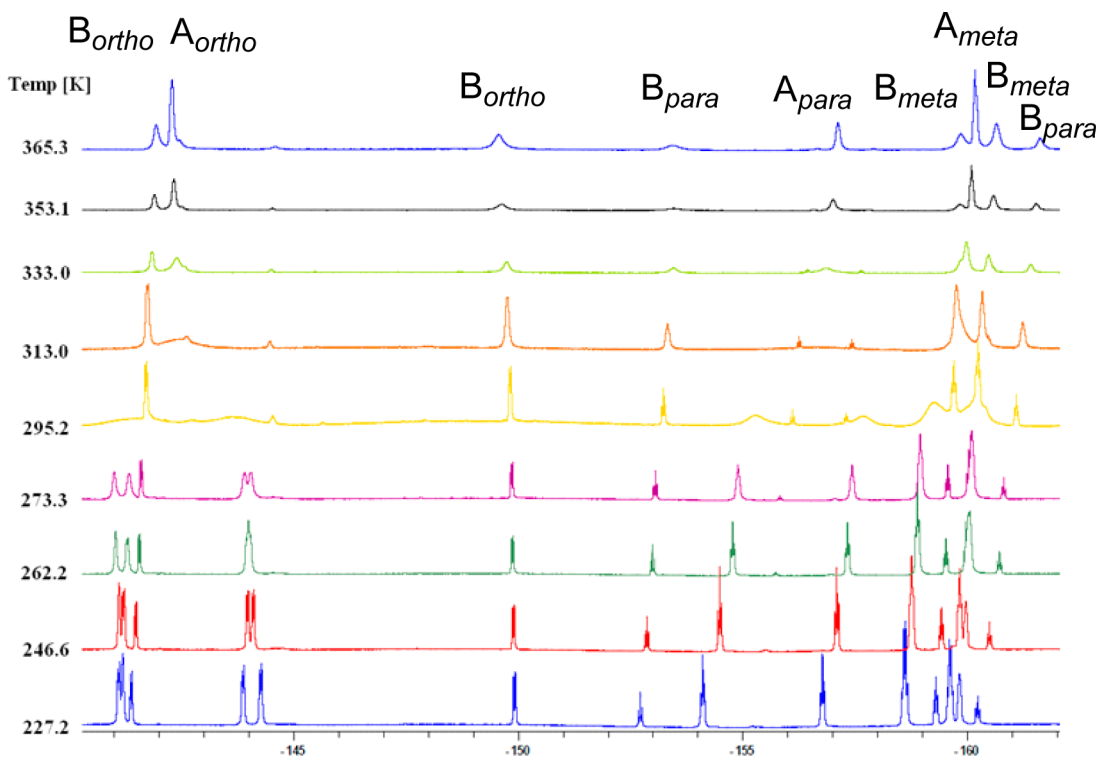


Figure 9. Variable-temperature ^{19}F NMR spectra for complex **11**. The labels in the spectrum correspond to the different fluorine atoms as defined in Figure 11.

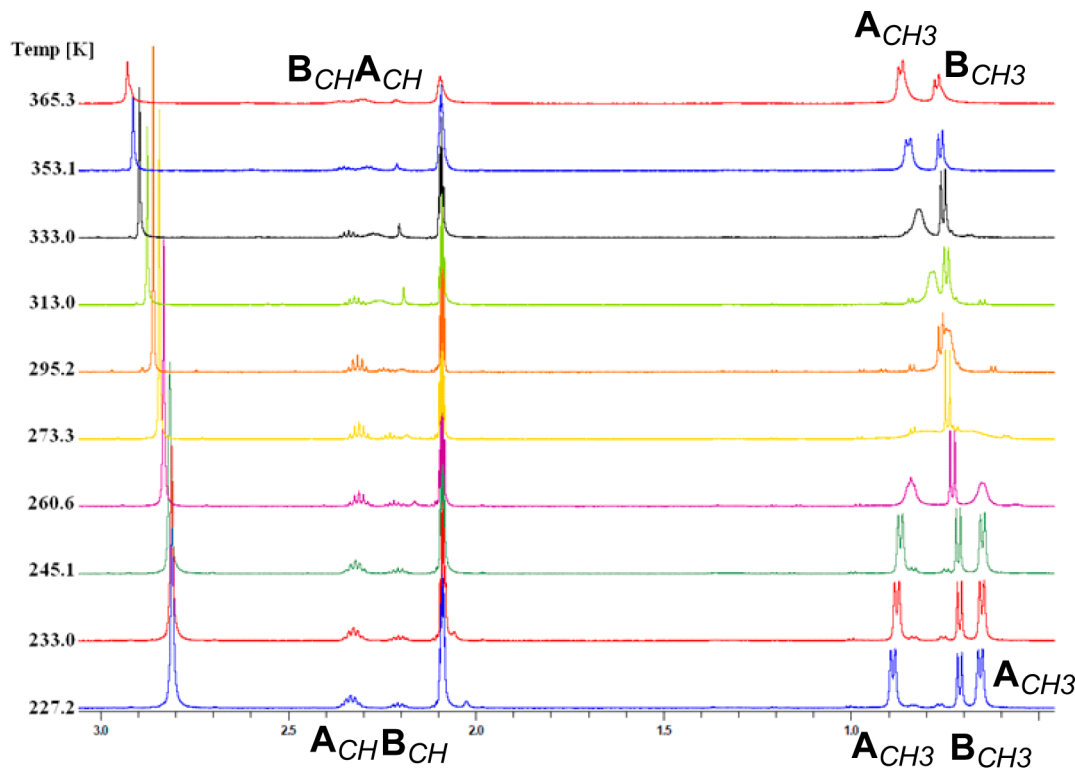


Figure 10. Variable-temperature ^1H NMR for complex **11**. The labels in the spectrum correspond to the different atoms in the corresponding complexes as defined in Figure 11.

alumoxane (MAO) in a 1:1000 ratio in toluene. The polymerizations were performed with an excess of propylene at room temperature for 3 h (Table 2). The precatalyst **11** exhibits an activity of $97 \text{ kg mol}^{-1} \text{ h}^{-1}$ at room temperature,

while complex **12** showed a similar reactivity of $113 \text{ kg mol}^{-1} \text{ h}^{-1}$, but only at elevated temperature (60°C), since at room temperature no polymerization was obtained. Unlike the case for the benzamidinates, no stereospecific fraction was obtained,

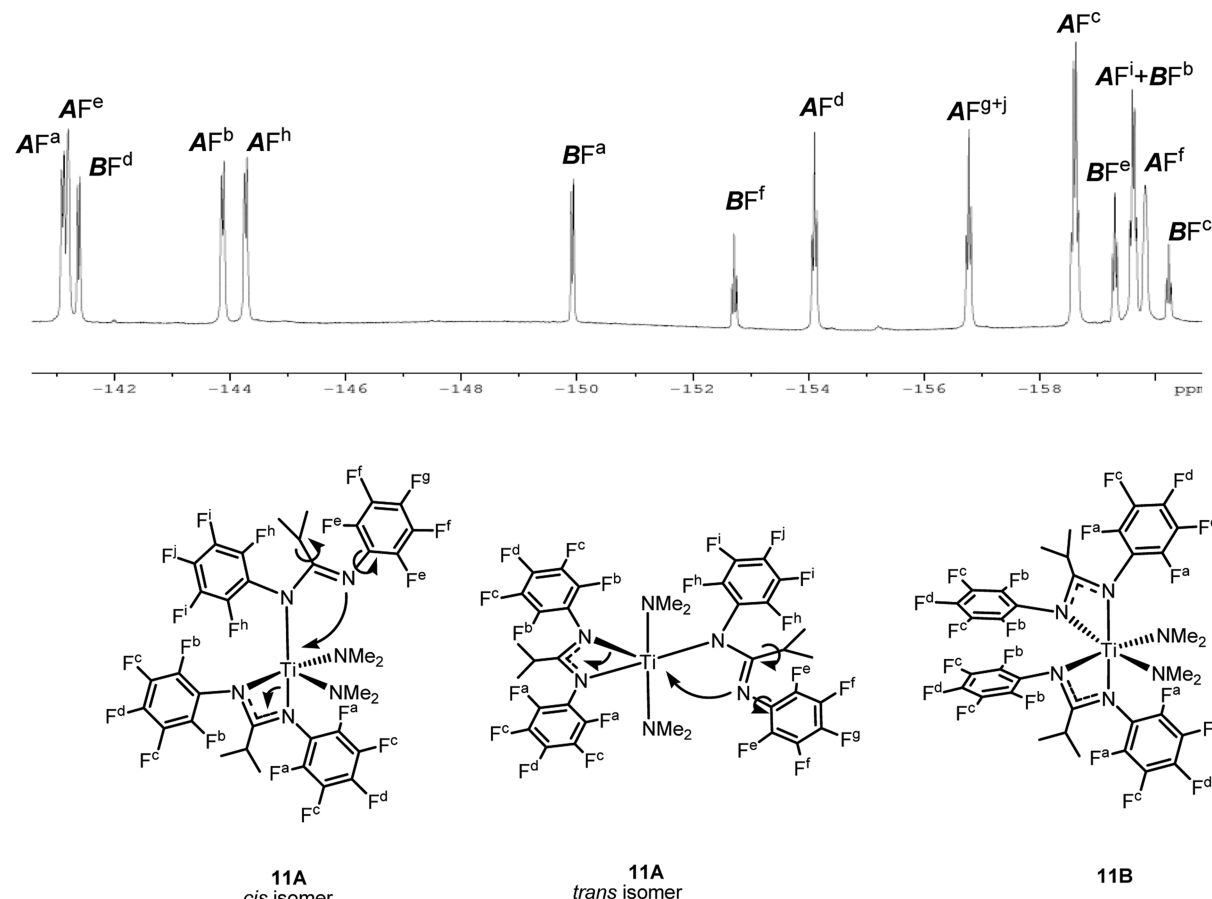


Figure 11. Assignment of fluorine atoms in **11A** (both plausible isomers) and **11B** at 227.2 K.

Table 1. Integration of H and F (Ortho) Atoms of Species 11A,B at the Lowest and the Highest Temperatures with No Coalescences^a

| temp (K) | ¹ H NMR | | ¹⁹ F NMR | |
|-------------|---|-------------|---------------------------------|---------------------------|
| | group | integration | group | integration |
| 227.2 | A(CH), B(CH) | 1.00, 0.31 | B(Fd), B(Fa) | 0.628, 0.654 |
| | A(CH ₃), B(CH ₃) | 3.00, 1.84 | A(Fa), A(Fb), A(Fe), A(Fh) | 1.03, 1.00, 1.03, 1.01 |
| 365.3 | A(CH), B(CH) | 1.00, 0.35 | B(ortho) left, B(ortho) left | 1.00, 1.01 |
| | A(CH ₃), B(CH ₃) | 5.87, 1.94 | A(ortho) | 3.15 |

^aThe legends at the spectrum correspond to the different atoms in the corresponding complexes as defined in Figure 11.

presumably due to the dynamic behavior of the complex **11A** forming various active species, as corroborated by the large molecular weight distribution of the obtained polymers. The *mmmm* pentad frequency (6–7%) was found in all cases, and in some cases the polymers were obtained as elastomeric materials, due to their molecular weight.¹⁶ The polymers that were obtained with complex **12** were atactic, and due to their low molecular weight, the consistency of these resulting materials was a tacky liquid. End group analysis has revealed that β -H-elimination/transfer to a monomer is responsible for the chain transfer process.

Interestingly, introduction of a fluorine atom at the meta position in complex **8** causes the formation of polypropylene

with a higher molecular weight as compared to that for complex **7**, presumably due to chain transfer suppression, whereas the *p*-fluorine complex **9** induces a higher insertion rate as compared to complex **7**. The most interesting result is obtained with the fluoronaphthyl complex **10**, which exhibits low activity but affords high-molecular-weight polymer, suggesting that the interaction of the fluorine atom with the metal center or the growing chain may be impeding chain termination as well as monomer insertion.

CONCLUSIONS

In this work we reported a series of new fluorinated titanium and zirconium bis(amidinates). Variable-temperature ¹H NMR revealed the dynamic behavior of the titanium complex **11A** with rearrangement of the ligand about the metal center. The dynamic behavior of the resulting fluorinated zirconium and titanium bis(amidinates) leads to the complete loss of *C*₂ symmetry followed by loss of stereospecificity in the polymerization of propylene. Substitution with fluorine atoms on different positions of the N-aryl substituent revealed that fluorine atoms at the meta position suppress termination of the growing chain, while *p*-F accelerates the insertion of monomer.

EXPERIMENTAL SECTION

All manipulations of air-sensitive materials were carried out with the rigorous exclusion of oxygen and moisture in oven-dried or flamed Schlenk-type glassware on a dual-manifold Schlenk line or interfaced to a high-vacuum (10^{-5} Torr) line or in a nitrogen-filled glovebox (M. Braun) with a medium-capacity recirculator (1–2 ppm O₂). Argon and nitrogen were purified by passage through a MnO oxygen removal

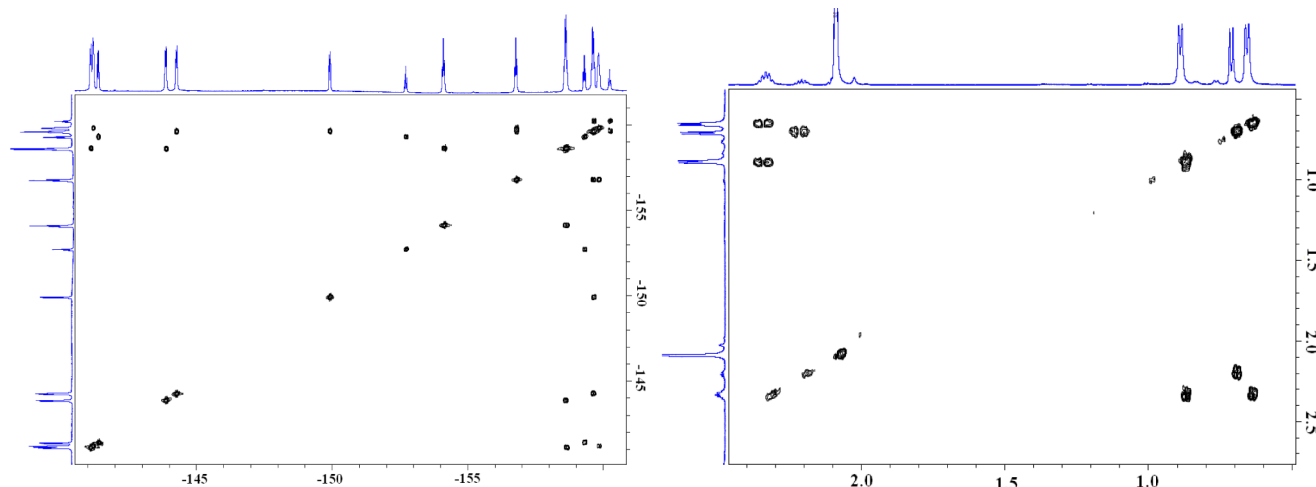


Figure 12. ^{19}F COSY (left) and ^1H COSY (right) of complex 11 at 227.2 K.

Table 2. Propylene Polymerization Results with the Bis(amidinate)dimethylamido Titanium and Zirconium Complexes 7–12^a

| precat. | activity ^b | M_w | PD | R_i | R_f |
|-----------------|-----------------------|----------------------|-----|----------------------|----------------------|
| 11 | 97.0 | 251 000 ^c | 8.3 | 2.4×10^{-3} | 3.4×10^{-5} |
| 7 | 33.5 | 55 000 | 3.9 | 1.3×10^{-3} | 3.9×10^{-5} |
| 8 | 35.0 | 142 500 | 3.9 | 1.3×10^{-3} | 1.5×10^{-5} |
| 9 | 63.2 | 82 000 | 3.7 | 2.5×10^{-3} | 4.7×10^{-5} |
| 10 | 1.7 | 82 000 | 2.6 | 5.2×10^{-5} | 6.6×10^{-8} |
| 10 ^d | 4.9 | 91 500 | 4.4 | 1.3×10^{-4} | 2.7×10^{-6} |
| 12 ^d | 113.0 | 4 500 | 4.5 | 3.1×10^{-3} | 1.3×10^{-3} |

^aReaction conditions: catalyst:MAO 1:1000 in 6 mL of toluene, 30 mL of propylene, room temperature, 3 h. ^bActivity in kg (mol of catalyst)⁻¹ h⁻¹. ^cBimodal signal in GPC analysis. ^dPolymerization temperature 60 °C.

column and a Davison 4 Å molecular sieve column. Analytically pure CH_2Cl_2 and CDCl_3 were used without any purification, and all other solvents (toluene, hexane, toluene- d_8 , C_6D_6) were dried over Na/K alloy, degassed by three freeze-pump-thaw cycles and vacuum-transferred prior to use. The final products 1–6 are air stable and do not need to be stored under inert conditions. All anilines and hexamethyldisiloxane (TMS_2O) were purchased from Sigma-Aldrich and used without further purification. $\text{Ti}(\text{NMe}_2)_4$, $\text{Zr}(\text{NMe}_2)_4$ ¹⁷ and 8-fluoronaphthalen-1-ylamine¹⁸ were prepared by literature procedures. NMR spectra were recorded on a Bruker Avance 300 spectrometer. NMR spectra for variable-temperature experiments were recorded on a Bruker Avance 600 spectrometer; the temperature was calibrated with MeOH (low temperature) and ethylene glycol (high temperature). ^1H and ^{13}C chemical shifts are referenced to internal solvent resonances and reported relative to TMS. ^{19}F chemical shifts were referenced according to IUPAC recommendations.¹⁹ The experiments with metal complexes were conducted in Teflon-sealed NMR tubes (J. Young) after the preparation of the sample under

Table 3. Crystallographic Data for Amidine Ligands 3–5 and Imidazole 6

| | amidine 3 | amidine 4 | amidine 5 | imidazole 6 |
|--|--|--|--|---|
| empirical formula | $\text{C}_{16}\text{H}_{16}\text{F}_2\text{N}_2$ | $\text{C}_{24}\text{H}_{20}\text{F}_2\text{N}_2$ | $\text{C}_{16}\text{H}_8\text{F}_{10}\text{N}_2$ | $\text{C}_{16}\text{H}_7\text{F}_9\text{N}_2$ |
| formula wt | 274.31 | 374.42 | 418.24 | 398.24 |
| T (K) | 293(2) | 293(2) | 293(2) | 293(2) |
| λ (Å) | 0.710 73 | 0.710 73 | 0.710 73 | 0.710 73 |
| cryst syst | triclinic | triclinic | monoclinic | monoclinic |
| space group | $P\bar{1}$ | $P\bar{1}$ | $P2_1/c$ | $C2/c$ |
| a (Å) | 8.579(2) | 11.659(2) | 8.029(2) | 16.809(3) |
| b (Å) | 11.799(2) | 11.707(3) | 12.698(2) | 16.277(3) |
| c (Å) | 14.702(3) | 15.017(3) | 16.824(3) | 11.616(2) |
| α (deg) | 101.20(3) | 93.24(2) | 97.21(3) | 99.09(3) |
| β (deg) | 90.71(3) | 112.97(3) | 97.21(3) | 99.09(3) |
| γ (deg) | 91.07(3) | 100.56(3) | 97.21(3) | 99.09(3) |
| V (Å ³) | 1459.4(5) | 1993.4(7) | 1701.7(6) | 3138.2(10) |
| Z | 4 | 4 | 4 | 8 |
| ρ (g/cm ³) | 1.248 | 1.248 | 1.633 | 1.686 |
| $\mu(\text{Mo K}\alpha)$ (mm ⁻¹) | 0.092 | 0.086 | 0.175 | 0.176 |
| R1, wR2 ($I > 2\sigma(I)$) | 0.0536, 0.1350 | 0.0750, 0.1898 | 0.0489, 0.1258 | 0.0457, 0.1155 |
| R1, wR2 (all data) | 0.0831, 0.1482 | 0.1616, 0.2191 | 0.1113, 0.1494 | 0.0936, 0.1322 |
| GOF on F^2 | 1.052 | 1.051 | 0.915 | 0.94 |
| $F(000)$ | 576 | 784 | 832 | 1584 |
| θ range for data collecn (deg) | 2.03–25.02 | 1.65–24.96 | 2.44–25.86 | 2.35–25.01 |
| no. of collected/unique rflns | 14 056/5121 | 15 985/6911 | 12 426/3166 | 2769/2769 |
| largest diff peak, hole (e/Å ³) | 0.131, -0.167 | 0.449, -0.185 | 0.268, -0.215 | 0.164, -0.132 |

Table 4. Crystallographic Data for Complexes 7, 9, 11, and 12

| | complex 7 | complex 9 | complex 11 | complex 12 |
|---|---|--|---|---|
| empirical formula | C ₃₆ H ₄₆ N ₆ Ti | C ₅₄ H ₆₃ F ₆ N ₉ Ti _{1.50} | C ₃₆ H ₂₆ F ₂₀ N ₆ Ti | C ₁₈ H ₁₃ F ₁₀ N ₃ Zr _{0.50} |
| formula wt | 610.69 | 1023.98 | 970.53 | 506.92 |
| T (K) | 293(2) | 240(2) | 240(2) | 240(2) |
| λ (Å) | 0.710 73 | 0.710 73 | 0.710 73 | 0.710 73 |
| cryst syst | monoclinic | triclinic | monoclinic | monoclinic |
| space group | P2 ₁ /c | P <bar{1}< td=""><td>C2/c</td><td>C2/c</td></bar{1}<> | C2/c | C2/c |
| a (Å) | 16.370(3) | 11.411(2) | 11.929(2) | 12.079(2) |
| b (Å) | 10.527(2) | 19.071(4) | 17.908(3) | 17.913(4) |
| c (Å) | 20.018(4) | 26.934(5) | 18.271(4) | 18.634(4) |
| α (deg) | | 101.71(3) | | |
| β (deg) | 98.81(3) | 97.29(3) | 98.15(3) | 98.97(3) |
| γ (deg) | | 100.20(3) | | |
| V (Å ³) | 3408.9(11) | 5567.4(18) | 3863.7(12) | 3982.6(14) |
| Z | 4 | 4 | 4 | 8 |
| ρ (g/cm ³) | 1.19 | 1.222 | 1.668 | 1.691 |
| μ(Mo Kα) (mm ⁻¹) | 0.284 | 0.283 | 0.356 | 0.407 |
| R1, wR2 (I > 2σ(I)) | 0.0509, 0.1310 | 0.0866, 0.2483 | 0.0754, 0.1504 | 0.0428, 0.0920 |
| R1, wR2 (all data) | 0.0736, 0.1398 | 0.1403, 0.2695 | 0.2288, 0.1926 | 0.0727, 0.1011 |
| GOF on F ² | 1.056 | 0.949 | 0.846 | 0.928 |
| F(000) | 1304 | 2148 | 1944 | 2016 |
| θ range for data collecn (deg) | 2.06 to 25.02 | 1.70 to 25.02 | 2.07 to 25.00 | 2.05 to 25.05 |
| no. of collected/unique rflns | 19 688/5917 | 70 805/19 135 | 20 758/3242 | 19 661/3497 (R(int) = 0.098) |
| largest diff peak, hole (e/Å ³) | 0.483, -0.341 | 0.923, -0.407 | 0.519, -0.359 | 0.268, -0.871 |

anaerobic conditions, with dried toluene-d₈ or C₆D₆. The molecular weights and polydispersities of the polymers were determined by the gel permeation chromatography (GPC) method on a Varian PL-GPC 220 instrument using 1,2,4-trichlorobenzene as the mobile phase at 160 °C. Polystyrene standards were used for the standard calibration curve of GPC.

X-ray Crystallographic Measurements. The single-crystal material was immersed in Paratone-N oil and was quickly fished with a glass rod and mounted on a Kappa CCD diffractometer under a cold stream of nitrogen. Data collection was performed using monochromated Mo Kα radiation using φ and ω scans to cover the Ewald sphere.²⁰ Accurate cell parameters were obtained with the amount of indicated reflections (Tables 3 and 4).²¹ The structure was solved by SHELXS-97 direct methods²² and refined by the SHELXL-97 program package.²³ The atoms were refined anisotropically. Hydrogen atoms were included using the riding model. Software used for molecular graphics: Mercury 2.4. The cell parameters and refinement data are presented in Tables 3 and 4.

Synthesis of PPSE. A mixture of 14.2 g of phosphorus pentoxide (P₂O₅), 25.6 g of hexamethylsiloxane (TMS₂O), and 30 mL of CH₂Cl₂ was refluxed for 30 min under a slow flow of N₂. After the mixture became a colorless liquid, the flask was placed under vacuum and slowly heated to 160 °C. The resulting viscous oil was used immediately for the synthesis of the corresponding amidine.

General Procedure for the Synthesis of Amidines. To the PPSE prepared from 14.2 g of P₂O₅ at 180 °C under an N₂ flow was added 1 equiv (1.25 mmol) of isobutyric acid, and the mixture was stirred for 5 min; during this time the reaction was heated to 200 °C. Two equivalents (2.5 mmol) of the corresponding aniline was then added dropwise with syringe to the reaction mixture, and the resulting viscous liquid was stirred at this temperature for 5 h. After that time the reaction mixture was made strongly basic (pH about 12) by adding a 1 M solution of NaOH. The resulting biphasic mixture was extracted three times with CH₂Cl₂; the combined organic fractions were washed with water, dried over Na₂SO₄, filtered and all volatiles removed under reduced pressure. The resulting crude product was purified by column chromatography on silica using a 1/1 hexane/CH₂Cl₂ mixture as eluent. Alternatively, the crude mixture may be separated by silica gel chromatography using 80/20 hexane/ethyl acetate as eluent.

1 (amidine): yield 85.2%; ¹H NMR (CDCl₃) δ 7.27–7.163 (5H, m), 6.98–6.84 (5H, m), 5.72 (1H, br), 2.84 (1H, m, ³J = 6.87 Hz), 0.71 (6H, d, ³J = 6.87 Hz); ¹³C NMR δ 158.2, 150.7, 140.6, 128.9, 128.5, 122.2, 121.5, 119.3, 29.0, 19.9.

2 (amidine): yield 89.8%; ¹H NMR (tol-d₈) δ 7.02 (4H, m), 6.71 (4H, m), 5.76 (1H, br), 2.76 (1H, sept, ³J = 7.32 Hz), 0.72 (6H, d, ³J = 7.33 Hz); ¹⁹F NMR δ -112.85 (1F, s), -111.81 (1F, s); ¹³C NMR δ 164.4, 159.3, 151.8, 141.5, 129.9, 117.0, 114.6, 109.1, 108.9, 108.3, 106.7, 29.5, 20.7.

3: yield 91.5%; ¹H NMR (CDCl₃) δ 7.29 (4H, t, ³J = 7.65 Hz), 7.02 (2H, t, ³J = 7.53 Hz), 6.84 (2H, t, ³J = 7.6 Hz), 6.09 (1H, br), 2.94 (1H, sept, ³J = 6.03 Hz), 0.85 (6H, d, ³J = 6.06 Hz); ¹⁹F NMR δ -122.72 (1F, s), -120.27 (1F, s); ¹³C NMR δ 171.9, 159.3, 150.1, 140.5, 137.1, 129.0, 122.5, 121.4, 119.5, 29.3, 20.0.

4: yield 83.5%; ¹H NMR (CDCl₃) δ 9.75 (1H, br) 7.55 – 6.73 (12H, m), 2.98 (1H, sept, ³J = 6.92 Hz), 1.12 (6H, d, ³J = 6.92 Hz); ¹⁹F NMR δ -112.85 (1F, s), -111.81 (1F, s); ¹³C NMR δ 175.2, 160.2, 157.8, 136.4, 136.4, 132.5, 132.5, 127.1, 125.4(d, ¹J = 10.25 Hz), 125.2 (d, ¹J = 3.32 Hz), 123.7, 118.7, 111.2, 110.9, 37.3, 19.5.

5 (amidine): yield 28%; ¹H NMR (CDCl₃) δ 4.80 (broad, 1H), 2.19 (sept, ³J = 6.9 Hz), 0.71 (d, ³J = 6.9 Hz); ¹⁹F NMR δ -165.50 (1F, t, ³J = 22.92 Hz), -164.64 (2F, t, ³J = 20.78 Hz), -164.10 (2F, t, ³J = 20.25 Hz), -157.64 (1F, t, ³J = 22.38 Hz), -154.20 (2F, d, ³J = 21.32 Hz), -146.09 (2F, d, ³J = 21.29 Hz); ¹³C NMR δ 165.2, 145.4–136.4 (C-Fs, low broad signals), 30.9, 19.4. Anal. Calcd for C₁₆H₈F₁₀N₂: C, 45.95; H, 1.93; N, 6.70. Found: C, 46.33; H, 1.95; N, 6.40.

6 (imidazole): yield 69%; ¹H NMR (CDCl₃) δ 1.06 (6H, d, ³J = 6.82 Hz), 1.99 (1H, m, ³J = 6.87 Hz); ¹⁹F NMR (CDCl₃) δ -164.10 (2F, t, ³J = 22.61 Hz), -164.07 (1F, t, ³J = 19.21 Hz), -163.39 (1F, q, ³J = 22.65 Hz), -157.19 (1F, q, ³J = 22.67 Hz), -154.20 (1F, d, ³J = 21.32 Hz), -153.21 (1F, d, ³J = 22.17 Hz), -145.65 (2F, d, ³J = 19.17 Hz); ¹³C NMR δ 162.3, 145.4–136.4 (C-Fs, low broad signals), 26.5, 20.5. Anal. Calcd for C₁₆H₇F₉N₂: C, 48.26; H, 1.77; N, 7.03. Found: C, 48.15; H, 1.68; N, 6.89.

General Procedure for the Synthesis of L₂M(NMe₂)₂ Complexes (7–12). A toluene solution of 2 equiv (0.88 mmol) of the corresponding ligand was added dropwise to a solution of 1 equiv of M(NMe₂)₄ (0.44 mmol) in toluene at room temperature, and the reaction mixture was stirred overnight. After this period of time all

volatiles were removed under reduced pressure, and to the resulting residue was added hexane, causing precipitation of solid material. The mixture was filtered, the resulting cake was washed with hexane, and the resulting solid was dried in *vacuo* to give the complexes as pure products. X-ray-quality crystals were obtained by slow evaporation of toluene from the toluene/complex solution, unless stated otherwise.

7: yield 87.3%; ¹H NMR (tol-*d*₈) δ 7.18 (4H, t, ³J = 7.74 Hz), 7.07 (4H, br), 6.96 (2H, t, ³J = 7.15), 3.07 (12H, s), 2.95 (2H, m, ³J = 7.22), 0.91 (12H, d, ³J = 7.22 Hz); ¹³C NMR δ 174.4, 149.2, 137.5, 126.5, 123.4, 121.6, 47.5, 30.7. Anal. Calcd for C₃₆H₄₆N₆Ti: C, 70.57; H, 7.90; N, 13.72. Found: C, 70.21; H, 7.28; N, 12.08.

8: yield 91.5%; ¹H NMR (tol-*d*₈) δ 6.99 (8H, m, ³J = 7.65 Hz), 6.79 (8H, m, ³J = 8.24 Hz), 3.11 (12H, s), 2.94 (2H, sept, ³J = 7.08 Hz), 0.90 (12H, d, ³J = 7.06 Hz); ¹⁹F NMR δ -113.02 (2F, q, ³J = 8.68 Hz); ¹³C NMR δ 174.6, 165.8, 160.9, 150.3, 150.1, 129.5, 129.3, 47.0, 20.4. Anal. Calcd for C₃₆H₄₂F₄N₆Ti: C, 63.16; H, 6.48; N, 12.28. Found: C, 61.66; H, 6.26; N, 11.34.

9: yield 86.7%; ¹H NMR (tol-*d*₈) δ 6.92 (8H, br), 3.16 (12H, s), 2.88 (2H, sept, ³J = 7.34 Hz), 0.89 (12H, d, ³J = 7.35 Hz); ¹⁹F NMR δ -119.83; ¹³C NMR δ 174.8, 162.0, 157.2, 144.6, 144.2, 115.3, 114.8, 47.1, 30.2, 20.5. Anal. Calcd for C₃₆H₄₂F₄N₆Ti: C, 63.16; H, 6.48; N, 12.28. Found: C, 62.11; H, 7.10; N, 11.52.

10: yield 92.3%; ¹H NMR (tol-*d*₈): δ 0.99 (12H, d, ³J = 6.94 Hz), 2.29 (2H, s), 2.91 (12H, m, ³J = 6.9 Hz), 7.448–6.733 (24H, m); ¹⁹F NMR δ -111.39 (dd, ³J = 12.87 Hz, ⁴J = 4.37 Hz); ¹³C NMR δ 172.81, 162.80, 162.16, 158.0, 157.3, 145.9, 137.5, 136.9, 136.9, 135.7, 128.3, 127.8, 125.6, 124.9, 124.2, 121.6, 121.4, 118.4, 117.3, 110.6, 110.17, 31.0, 20.0. Anal. Calcd for C₅₂H₅₀F₃N₆Ti: C, 70.58; H, 5.92; N, 9.50. Found: C, 76.58; H, 6.54; N, 10.11.

11: yield 84.0%; X-ray-quality crystals obtained by cooling the saturated toluene solution from 50 °C to room temperature; ¹H NMR (C₆D₆) δ 2.86 (s, 12H), 2.32 (sept, ³J = 7.2 Hz, 2H), 0.74 (d, ³J = 7.2 Hz, 12H); ¹⁹F NMR spectrum at room temperature consists of broad signals that cannot be assigned properly; ¹³C NMR δ 179.6, 45.1, 31.5, 17.4. Anal. Calcd for C₃₆H₂₈F₂₀N₆Ti: C, 44.46; H, 2.90; N, 8.64. Found: C, 44.93; H, 2.56; N, 8.17.

12: yield 76.2% ¹H NMR (C₆D₆) δ 2.59 (s, 12H), 2.33 (sept, ³J = 6.9 Hz, 2H), 0.74 (d, ³J = 6.9 Hz, 12H); ¹⁹F NMR δ -148.5 (d, ³J = 21.5 Hz, 8F), -160.30 (t, ³J = 21.7 Hz, 4F), -163.87 (t, ³J = 18.9 Hz, 8F); ¹³C NMR δ 184.6, 40.3, 32.6, 19.4. Anal. Calcd for C₃₆H₂₈F₂₀N₅Zr: C, 42.56; H, 2.78; N, 8.27. Found: C, 44.93; H, 2.30; N, 6.89.

Typical Procedure for Propylene Polymerization. Inside the glovebox, 10 mg of the complex, the appropriate amount of the MAO (1:1000 metal:Al ratio), and 6 mL of toluene were mixed and loaded into a stainless steel reactor. The reactor was connected to the high-vacuum line, and 30 mL of propylene was transferred into the reactor. The reaction mixture was warmed to the desired temperature and stirred for 3 h. The reaction was quenched with acetylacetone, and the resulting polymer was washed with methanol followed by acetone. The solvents were dried out in the vacuum oven at 50 °C. The resulting material was fractionalized with hexane in a Soxhlet apparatus.

■ ASSOCIATED CONTENT

S Supporting Information

Figures, tables, and CIF files giving an Eyring plot for the dynamic process in complex **11**, COSY of complex **11** at high (365 K) and low (227 K) temperatures, and crystallographic data for ligands **3–6** and complexes **7, 9, 11**, and **12**. This material is available free of charge via the Internet at <http://pubs.acs.org>.

■ AUTHOR INFORMATION

Corresponding Author

*E-mail: chmoris@tx.technion.ac.il

Notes

The authors declare no competing financial interest.

■ ACKNOWLEDGMENTS

This research was supported by the USA-Israel Binational Science Foundation under Contract 2008283. S.A. thanks Raymond Rosen for his fellowship.

■ REFERENCES

- (1) Kissin, Y. V. *Alkene Polymerization Reactions with Transition Metal Catalysts*, 1st ed.; Elsevier: Amsterdam, 2008; Studies in Surface Science and Catalysis Vol. 173, pp 28–29 and references therein.
- (2) (a) Lamberti, M.; Mazzeo, M.; Pappalardo, D.; Pellecchia, C. *Coord. Chem. Rev.* **2009**, *293*, 2082–2097. (b) Takeuchi, D. *Dalton Trans.* **2010**, *39*, 311–328. (c) Baugh, L. S.; Canich, J.-A. M. In: *Stereoselective Polymerization with Single-Site Catalysts*; CRC Press: Boca Raton, FL, 2008. (d) Givson, V. C.; Redshaw, C.; Solan, G. A. *Chem. Rev.* **2007**, *107*, 1745–1776.
- (3) (a) Delferro, M.; Marks, T. J. *Chem. Rev.* **2011**, *111*, 2450–2485 and references therein. (b) Gibson, V. C.; Spitzmesser, S. K. *Chem. Rev.* **2003**, *103*, 283–316. (c) Makio, H.; Fujita, T. *Acc. Chem. Res.* **2009**, *42*, 1532–1544. (d) Amin, S. B.; Marks, T. J. *Angew. Chem., Int. Ed.* **2008**, *47*, 2006–2025. (e) Vanka, K.; Xu, Z.; Seth, M.; Ziegler, T. *Top. Catal.* **2005**, *34*, 143–164.
- (4) (a) Edelmann, F. T. *Adv. Organomet. Chem.* **2008**, *57*, 183–352. (b) Collins, S. *Coord. Chem. Rev.* **2011**, *255*, 118–138. (c) Edelmann, F. T. *Struct. Bonding (Berlin)* **2010**, *137*, 109–163.
- (5) (a) Volkis, V.; Shmulinson, M.; Averbuj, C.; Lisovskii, A.; Edelmann, F. T.; Eisen, M. S. *Organometallics* **1998**, *17*, 3155–3157. (b) Sita, L. R.; Babcock, J. R. *Organometallics* **1998**, *17*, 5228–5230. (c) Zhang, Y.; Sita, L. R. *Chem. Commun.* **2003**, 2358–2359. (d) Kissounko, D. A.; Zabalov, M. V.; Brusova, G. P.; Lemenovskii, D. A. *Russ. Chem. Rev.* **2006**, *75*, 351–374.
- (6) Volkis, V.; Nelkenbaum, E.; Lisovskii, A.; Hasson, G.; Semiat, R.; Kapon, M.; Botoshansky, M.; Eishen, Y.; Eisen, M. S. *J. Am. Chem. Soc.* **2003**, *125*, 2179–2194.
- (7) (a) Volkis, V.; Lisovskii, A.; Tumanskii, B.; Shuster, M.; Eisen, M. S. *Organometallics* **2006**, *25*, 2656–2666. (b) Aharonovich, S.; Volkis, V.; Eisen, M. S. *Macromol. Symp.* **2007**, *260*, 165–171.
- (8) (a) Volkis, V.; Aharonovich, S.; Eisen, M. S. *Macromol. Res.* **2010**, *18*, 967–973. (b) Volkis, V.; Lisovskii, A.; Tumanskii, B.; Shuster, M.; Eisen, M. S. *Organometallics* **2006**, *25*, 2656–2666.
- (9) (a) Aharonovich, S.; Botoshansky, M.; Balazs, Y. S.; Eisen, M. S. *Organometallics* **2012**, *31*, 3435–3438. (b) Aharonovich, S. *Hetero-aza-allyl Complexes of Li, Ti, Zr, and V: Structure, Reactivity and Catalytic Propylene Polymerization*. Ph.D. Thesis, Technion—Israel Institute of Technology, 2010.
- (10) (a) Brylikov, K. P. *Russ. Chem. Rev.* **2007**, *81*, 253–277 and references therein. (b) Nokata, N.; Toda, T.; Ishii, A. *Polym. Chem.* **2011**, *2*, 1597–1610.
- (11) (a) Kawai, K.; Fujita, T. *Top. Organomet. Chem.* **2009**, *26*, 3–46. (b) Mitani, M.; Saito, J.; Ishii, S.; Nakayama, Y.; Makio, H.; Matsukawa, N.; Matsui, S.; Mohri, J.; Furuyama, R.; Terao, H.; Bando, H.; Tanaka, H.; Fujita, T. *Chem. Rec.* **2004**, *4*, 137–158. (c) Sakuma, A.; Weiser, M. S.; Fujita, T. *Polym. J.* **2007**, *39*, 193–207. (d) Makio, H.; Fujita, T. *Bull. Chem. Soc. Jpn.* **2005**, *78*, 52–66. For other similar living systems see: (e) Tian, J.; Coates, G. W. *Angew. Chem., Int. Ed.* **2000**, *39*, 3626–3629. (f) Tian, J.; Hustad, P. D.; Coates, G. W. *J. Am. Chem. Soc.* **2001**, *123*, 5134–5135.
- (12) (a) Makio, H.; Fujita, T. *Acc. Chem. Res.* **2009**, *42*, 1532–1544. (b) Chan, M. C. W.; Kui, S. C. F.; Cole, J. M.; McIntyre, G. J.; Matsui, S.; Zhu, N.; Tam, K.-H. *Chem. Eur. J.* **2006**, *12*, 2607–2619. (c) Kui, S. C. F.; Zhu, N.; Chan, M. C. W. *Angew. Chem., Int. Ed.* **2003**, *42*, 1628–1632. (d) Weberski, M. P.; Chen, C.; Delferro, M.; Zuccaccia, C.; Macchioni, A.; Marks, T. J. *Organometallics* **2012**, *31*, 3773–3789.
- (13) Ogata, S.; Mochizuki, A.; Kakimoto, M.; Imai, Y. *Bull. Chem. Soc. Jpn.* **1986**, *59*, 2171–2177.
- (14) (a) Smolensky, E.; Kapon, M.; Woollins, J. D.; Eisen, M. S. *Organometallics* **2005**, *24*, 3255–3265. (b) Ward, B. D.; Risler, H.; Weitershaus, K.; Bellemin-Laponnaz, S.; Wadeohl, H.; Gade, L. H. *Inorg. Chem.* **2006**, *45*, 7777–7787. (c) Cortright, S. B.; Huffman, J.

- C.; Yoder, R. A.; Coalter, J. N.; Johnston, J. N. *Organometallics* **2004**, *23*, 2238–2250. (d) Dawson, D. M.; Walker, D. A.; Thornton-Pett, M.; Bochmann, M. *Dalton Trans.* **2000**, *4*, 459–466.
(15) Bondi, A. *J. Phys. Chem.* **1964**, *68*, 441–451.
(16) Resconi, L.; Jones, R. L.; Rheingold, A. L.; Yap, G. P. A. *Organometallics* **1996**, *15*, 998–1005.
(17) Bradley, D. C.; Thomas, I. M. *J. Chem. Soc.* **1960**, 3857–3861.
(18) Zhu, Zh.; Colby, N. L.; Lovdahl, M.; Mennen, K. E.; Acciaca, A.; Beylin, V. G.; Clark, J. D.; Belmont, D. T. *Org. Process Res. Dev.* **2007**, *11*, 907–909.
(19) Harris, R. K.; Becker, E. D.; Cabral De Menezes, S. M.; Goodfellow, R.; Granger, P. *Pure Appl. Chem.* **2001**, *73*, 1795–1818.
(20) *KappaCCD Server Software*; Nonius BV, Delft, The Netherlands, 1997.
(21) Otwinowski, Z.; Minor, W. *Methods Enzymol.* **1997**, *276*, 307.
(22) Sheldrick, G. M. *Acta Crystallogr., Sect. A: Found. Crystallogr.* **1990**, *A46*, 467.
(23) ORTEP, TEXSAN Structure Analysis Package; Molecular Structure Corp., The Woodlands, TX, 1999.